The Pan-STARRS 1 discoveries of five new neptune trojans

Lin, H. W., Chen, Y-T., Holman, M. J., Ip, W-H., Payne, M. J., Lacerda, P., Fraser, W. C., Gerdes, D. W., Bieryla, A., Sie, Z. F., Chen, W. P., Burgett, W. S., Denneau, L., Jedicke, R., Kaiser, N., Magnier, E. A., Tonry, J. L., Wainscoat, R. J., & Waters, C. (2016). The Pan-STARRS 1 discoveries of five new neptune trojans. *Astronomical Journal*, *152*(5), [147]. https://doi.org/10.3847/0004-6256/152/5/147

Published in:
Astronomical Journal

Document Version:
Publisher's PDF, also known as Version of record

The Astronomical Journal, 152:147 (8pp), 2016 November doi:10.3847/0004-6256/152/5/147

THE PAN-STARRS 1 DISCOVERIES OF FIVE NEW NEPTUNE TROJANS

Hsing Wen Lin (林省文)[1], Ying-Tung Chen (陳英同)[2], Matthew J. Holman[3,4], Wing-Huen Ip (葉永烜)[1,5], M. J. Payne[4], P. Lacerda[6], W. C. Fraser[6], D. W. Gerdes[7], A. Bieryla[4], Z.-F. Sie (謝宗富)[1], W.-P. Chen (陳文屏)[1], W. S. Burgett[8], L. Denneau[8], R. Jedicke[8], N. Kaiser[8], E. A. Magnier[8], J. L. Tonry[8], R. J. Wainscoat[8], and C. Waters[8]
[1] Institute of Astronomy, National Central University, 32001, Taiwan; edlin@gm.astro.ncu.edu.tw
[2] Institute of Astronomy and Astrophysics, Academia Sinica, P.O. Box 23-141, Taipei 106, Taiwan
[3] Harvard-Smithsonian Center for Astrophysics, 60 Garden Street, Cambridge, MA 02138, USA
[4] Center for Astrophysics, 60 Garden Street, Cambridge, MA 02138, USA
[5] Space Science Institute, Macau University of Science and Technology, Macau
[6] Astrophysics Research Centre, Queen's University Belfast, BT7 1NN, Northern Ireland, UK
[7] Department of Physics, University of Michigan, Ann Arbor, MI 48109, USA
[8] Institute for Astronomy, University of Hawaii at Manoa, Honolulu, HI 96822, USA
Received 2016 June 2; revised 2016 September 14; accepted 2016 September 14; published 2016 October 31

ABSTRACT

In this work, we report the detection of seven Neptune Trojans (NTs) in the Pan-STARRS 1 (PS1) survey. Five of these are new discoveries, consisting of four L4 Trojans and one L5 Trojan. Our orbital simulations show that the L5 Trojan stably librates for only several million years. This suggests that the L5 Trojan must be of recent capture origin. On the other hand, all four new L4 Trojans stably occupy the 1:1 resonance with Neptune for more than 1 Gyr. They can, therefore, be of primordial origin. Our survey simulation results show that the inclination width of the NT population should be between 7° and 27° at >95% confidence, and most likely ∼11°. In this paper, we describe the PS1 survey, the Outer Solar System pipeline, the confirming observations, and the orbital/physical properties of the new NTs.

Key words: Kuiper belt: general – minor planets, asteroids: general – surveys

1. INTRODUCTION

The best-known Trojans are the asteroids in a co-orbital 1:1 mean motion resonance with Jupiter. Those in stable libration around the Lagrange point 60° ahead of Jupiter are called L4 Trojans, and those around the Lagrange point 60° behind are called L5 Trojans. There are more than 6000 known Jovian Trojans with sizes $\gtrsim$10 km. Yoshida & Nakamura (2005) estimated that the total number of 1 km sized Jovian Trojans could be as many as 600,000. After Jupiter, Neptune has the second-largest population of Trojans. Prior to this study, nine L4 Neptune Trojans (or NTs) and three L5 NTs had been discovered (Elliot et al. 2005; Sheppard & Trujillo 2006, 2010b; Parker et al. 2013; Alexandersen et al. 2014; Gerdes et al. 2016).

Nesvorný & Dones (2002) examined the orbital evolution and long-term stability of Trojans of Saturn, Uranus, and Neptune, under the current planetary configuration. They found that unlike the cases of Saturn and Uranus, where their Trojans could be removed on relatively short timescales, the primordial population of NTs can survive to the present time after their formation. Subsequently, the first NT, 2001 QR_{322} at L4, was found in the Deep Ecliptic Survey (Elliot et al. 2005). Based on the low inclination (∼1°.3) of 2001 QR_{322} with a size of ∼100 km, Chiang & Lithwick (2005) proposed that large (∼100 km sized) NTs might be primordial objects formed in situ by accretion in a thin disk. This means that NTs should generally have $i \lesssim 10°$. Following the discovery of three more NTs, one of which has a high inclination (see Table 1, with a list of the known NTs and those detected in this study), Sheppard & Trujillo (2006) suggested that a thick cloud of high-inclination NTs, which could be of capture origin, should exist with a 4:1 ratio over the low-inclination population.

In the context of the Nice model (Gomes et al. 2005; Tsiganis et al. 2005), Morbidelli et al. (2005) investigated the chaotic capture of small bodies at the two Lagrangian points of Jupiter during the planetary migration phase. Following a similar approach, Nesvorný & Vokrouhlický (2009) produced a model calculation of the capture process of NTs. Although the inclinations of the objects captured from the thin solar nebula disk could be later increased by dynamical processes, the numerical results could not account for the 4:1 high-i to low-i NT ratio indicated by the observations of Sheppard & Trujillo (2006). This discrepancy might be worsened if the orbits of the planetesimals before chaotic capture were excited by the gravitational scattering effect of a population of Pluto-sized objects, according to these authors.

Parker (2015) applied a statistical method to debias the observed distributions of orbital inclinations, eccentricities, and libration amplitudes of NTs. His treatment confirmed the existence of the thick-cloud population with $\sigma_i > 11°$. Here σ_i is the inclination width of the Brown distribution (Brown 2001):

$$p(i) = \sin(i)\exp\left(-\frac{1}{2}(i/\sigma_i)^2\right)di. \quad (1)$$

From a numerical study of the resonant capture effect via planetary orbital migration, Parker (2015) showed that low-inclination objects can be captured into high-inclination NTs, but the conversion efficiency is too low to account for the presence of the high-inclination population. On the other hand, if the original planetesimals were characterized by high-inclination orbits, their NT counterparts captured into 1:1 resonance with Neptune could preserve their high inclinations and hence cause the formation of a thick NT cloud.

Chen et al. (2016) provided an alternative mechanism to effectively form the high-inclination NTs. They investigated how planetary migration affects the orbital elements' distribution of NTs and found that if orbital eccentricities and

Table 1
Barycentric Oscillating Orbital Elements of PS1-detected and Known NTs

Name	a (au)	e	i (deg)	Ω (deg)	ω (deg)	Peri. Date (JD)	Epoch (JD)	H	L	PS1 Detected	β[a]	λ[b]
2001 QR_{322}	30.233	0.0285	1.323	151.636	158.76	2444677	2452142.8	7.9	L4	yes	21.85	−1.05
2004 KV_{18}	30.353[c]	0.189	13.573	235.593	295.733	2446125.4	2453351.5	8.9	L5	⋯	⋯	⋯
385571 Otrera (2004 UP_{10})	30.184	0.027	1.431	34.780	358.452	2457945.4	2454668.5	8.8	L4	⋯	⋯	⋯
385695 (2005 TO_{74})	30.137	0.051	5.253	169.387	304.750	2470616.8	2454522.5	8.3	L4	⋯	⋯	⋯
2005 TN_{53}	30.171	0.064	24.988	9.278	85.892	2467102.2	2454775.5	9.0	L4	⋯	⋯	⋯
2006 RJ_{103}	30.038	0.0300	8.163	120.867	27.26	2475056	2453626.8	7.5	L4	yes	28.12	−8.42
2007 VL_{305}	30.004	0.062	28.125	188.611	215.518	2456036.1	2454566.5	7.9	L4	⋯	⋯	
2008 LC_{18}	30.090	0.079	27.489	88.528	6.845	2427000.1	2454759.5	8.4	L5	⋯	⋯	⋯
2010 TS_{191}	30.006	0.0457	6.563	129.600	299.5	2460637	2455476.9	7.9	L4	yes	36.07	−6.76
2010 TT_{191}	30.094	0.0701	4.276	249.295	7.8	2429839	2454419.0	7.9	L4	yes	54.76	1.18
2011 HM_{102}	30.119	0.081	29.389	100.993	152.287	2452480.3	2455758.5	8.1	L5	⋯	⋯	⋯
2011 SO_{277}	30.161	0.0118	9.639	113.528	117.7	2431675	2455831.0	7.6	L4	yes	16.19	−9.87
2011 WG_{157}	30.031	0.0278	23.299	352.165	215.3	2482896	2455885.8	7.0	L4	yes	41.95	18.06
2012 UV_{177}	30.175	0.074	20.811	265.753	200.784	2467673.8	2456131.5	9.2	L4	⋯	⋯	⋯
2013 KY_{18}	30.149	0.123	6.659	84.397	271.2	2471956	2456429.0	6.6	L5	yes	249.82	1.79
2014 QO_{441}	30.104	0.105	18.824	107.110	113.897	2429010.4	2456910.5	8.3	L4	⋯	⋯	
2014 QP_{441}	30.0785	0.067	19.394	96.626	2.639	2467286.1	2456979.5	9.3	L4	⋯	⋯	

Notes.
[a] The discovery ecliptic latitude.
[b] The discovery ecliptic longitude.
[c] The barycentric orbital elements of non-PS1-detected NTs were queried from the JPL HORIZONS system.

inclinations of Neptune and Uranus were damping during planetary migration, the secular resonances with Neptune will increase the probability of trapping the test particles into high-inclination NT orbits. Moreover, most primordial NTs, especially the high-inclination ones, were unstable and lost in the damping case. From these results, they concluded that the current existent NTs can be explained by the capture origin, particularly the trapping scenario with orbital damping of Neptune and Uranus during planet migration.

The first NT at L5, 2008 LC_{18}, was discovered by Sheppard & Trujillo (2010b). One more was found by Parker et al. (2013). According to Sheppard & Trujillo (2006) and Parker (2015), the difference in the numbers of known NTs in the L4 and L5 points, respectively, could be an observational bias caused by the fact that the L5 point of the NTs is currently in the vicinity of the Galactic center, making it difficult to clearly identify slowly moving foreground objects.

Due to the small number of known NTs, it has been difficult to reconstruct their size distribution and to estimate their total number. Chiang & Lithwick (2005) and Sheppard & Trujillo (2006) suggested that the number of large (size $>$ 65 km) NTs should exceed that of the Jovian Trojans by more than a factor of 10. Alexandersen et al. (2014) discovered one temporary and one stable NT and derived the populations of 210^{+900}_{-200} and 150^{+600}_{-140}, respectively, with $H \lesssim 10.0$. From an ultradeep, pencil-beam survey with a detection efficiency of 50% for objects with $R \sim 25.7$ mag, Sheppard & Trujillo (2010a) derived that the cumulative luminosity function of $m_R < 23.5$ mag follows a steep power law of index $\alpha \sim 0.8 \pm 0.2$:

$$\Sigma(m_R) = 10^{0.8(m_R - m_0)}. \quad (2)$$

In other words, the size frequency distribution of the bright NTs at size $a >$100 km has a power-law index $\sim 5 \pm 1$:

$$dN/da \propto a^{-5}. \quad (3)$$

For reference, Jovian Trojan populations, cold populations, and hot populations of Trans-Neptunian Objects (TNOs) have $\alpha \sim 1.0$, 1.5, and 0.87, respectively (Fraser et al. 2014). This clearly shows that the luminosity function of the NT population has a power-law index, α, similar to the Jovian Trojans and the hot population of TNOs. This result is an obvious interpretation from the fact that they all have the same size frequency distribution.

The long-term orbital stability of NTs has been studied by Nesvorný & Dones (2002), Dvorak et al. (2007), and Zhou et al. (2009, 2011), who showed that NTs can be stable for over 4 Gyr even with orbital inclinations ∼30°. However, the stable region is restricted in eccentricity ($e \lesssim 0.1$). The orbital stability of individual known NTs has been investigated by Brasser et al. (2004), Guan et al. (2012), Marzari et al. (2003), Horner & Lykawka (2010), Horner & Lykawka (2012), Horner et al. (2012), and Lykawka et al. (2009). In general, they can be classified into three different dynamical regimes:

1. Objects temporarily captured into unstable orbits: these kinds of NTs are located completely outside the stable region and have a dynamical lifetime as short as 1 Myr (Guan et al. 2012; Horner et al. 2012).
2. Objects in marginally stable orbits: these NTs are found near the edge of the stable region or in the proximity of the secular resonances with a dynamical lifetime of about 100 Myr (Horner & Lykawka 2010; Lykawka et al. 2011; Zhou et al. 2011).
3. Stable objects: they are located deep inside the stable region with a dynamical lifetime as long as the age of the solar system and could be of primordial origin.

Our current knowledge of the NTs is based on the discoveries by several different surveys (Elliot et al. 2005; Sheppard & Trujillo 2006, 2010b; Parker et al. 2013; Alexandersen et al. 2014; Gerdes et al. 2016). Without a

comprehensive full-sky survey to cover most of the Trojan clouds, it is difficult to estimate the total number, the size distribution, the orbital distribution, and the L4/L5 asymmetry of NTs. In comparison, the PS1 project covering the whole Northern Hemisphere to a limiting magnitude of $r_{P1} \sim 22$ presents an ideal opportunity to search for NTs with significant reduction in the latitudinal and longitudinal biases. In this paper, we report the detections of seven NTs by PS1, five of which are new discoveries.

This paper is organized as follows. Section 2 will introduce the PS1 survey and the Outer Solar System pipeline for searching for distant moving objects. In Section 3, we describe how to select the Trojan candidates, confirm them, and report the discoveries. In Section 4, we calculate the orbital and physical properties of the NTs. In Section 5, we describe how to perform the inclination debiasing of the PS1 survey and investigate the intrinsic inclination distribution of stable L4 NTs. In Section 6, we roughly estimate the luminosity function of stable L4 NTs. In Section 7, we discuss the ratio of high- and low-inclination populations of NTs and the possible asymmetry of L4 and L5 distributions. A summary is given in Section 8.

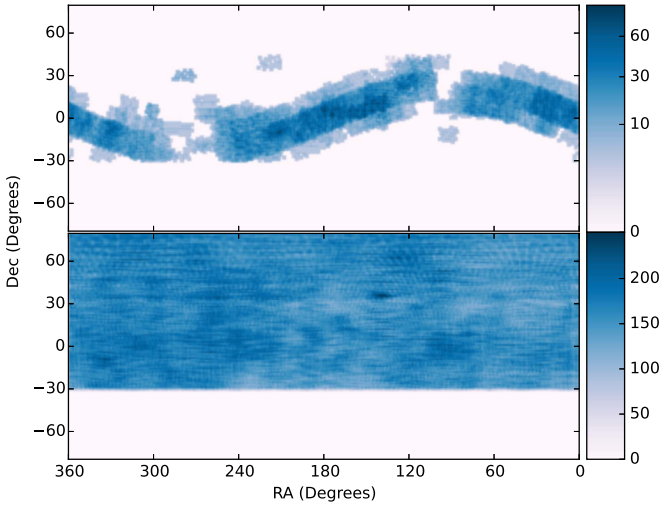

Figure 1. The sky coverage of the Solar System Survey (top) and 3π survey (bottom). The color bar shows the total number of exposures in all bands with the same pointing.

2. PAN-STARRS 1 SURVEY AND THE OUTER SOLAR SYSTEM PIPELINE

The PS1 Survey began in 2010 May and ended in 2014 May. With a 1.8 m Ritchey–Chretien reflector located on Haleakala, Maui, and a 1.4 gigapixel camera covering 7 square degrees on the sky, the PS1 telescope was able to observe the whole visible sky within a week, searching for all kinds of astrophysical transients and solar system moving objects.

The PS1 observations were taken using five different survey modes (Kaiser et al. 2010):

1. The 3π Steradians Survey, using the PS1 photometric system (Tonry et al. 2012), g_{P1} (bandpass ~400–550 nm), r_{P1} (~550–700 nm), i_{P1} (~690–820 nm), z_{P1} (~820–920 nm), and y_{P1} (~920–1100 nm), which is similar but not identical to the SDSS/Sloan system with the addition of y_{P1}.
2. The Solar System Survey, which is optimized for near-Earth asteroids and other solar system objects by covering the whole $\pm 10°$ and part of $\pm 20°$ areas of the ecliptic plane with the w_{P1}-band filter (400–820 nm), which is equivalent to $g_{P1} + r_{P1} + i_{P1}$.
3. The Medium Deep Survey, covering 10 selected fields and nightly observations with long exposures (113 s for g_{P1} and r_{P1}, 240 s for i_{P1}, z_{P1}, and y_{P1}) in each passband.
4. Stellar Transit Survey.
5. Deep Survey of M31 (Lee et al. 2012).

The w_{P1}-band Solar System Survey has contributed most to the discoveries of solar system minor bodies due to its optimized cadence for searching moving objects and deeper limiting magnitude of 22.5, which is about one magnitude more than the 3π survey. To demonstrate the sky coverage of PS1, we separate the entire sky into 360 (R.A.) × 180 (decl.) pixels, and each pixel is 1 square degree. Then we register the location of each pointing from the 3pi and Solar System Survey and assign it to a pixel location. We filled the eight pixels surrounding the center pixel, but then scale by a factor of 7/9, because of the 7 square degree field of view of PS1.

The approximate sky coverage of the 3π and Solar System Survey from 2010 to 2014 is illustrated in Figure 1. The concentration of the PS1 Solar System Survey within $\pm 10°$ and part of the area between $\pm 10°$ and $\pm 15°$ of the ecliptic plane are clearly shown. The PS1 data products will be released to the public in 2017.

The PS1 Outer Solar System Pipeline will be described fully in forthcoming papers by M. J. Holman et al. (2016, in preparation) and M. J. Payne & M. J. Holman (2016, in preparation). We used the PS1 Outer Solar System Pipeline to process the data and search for slow-moving solar system objects. The PS1 Outer Solar System Pipeline uses a distance-based approach for identifying and linking point-source detections. It begins with the source detection catalogs of direct images produced by the PS1 Image Processing Pipeline (IPP), rather than difference images. We avoid using difference-image source catalogs because either slow-moving objects are eliminated or their signal-to-noise ratios are significantly reduced, due to the short time interval (15 minute) between two consecutive exposures. In the next step, the pipeline develops a catalog of stationary objects for elimination in each exposure.

After the removal of the stationary sources, the pipeline will identify "tracklets," i.e., sequences of source detections in the same night that are consistent with linear motion in the constant rate. The pipeline evaluates the tracklets of moving objects by the goodness of fit, using estimated astrometric uncertainties. Finally, the pipeline links the tracklets over intervals ranging from a few nights to multiple years, allowing a full fit to be performed to characterize the orbital parameters.

3. IDENTIFICATION AND CONFIRMATION OF TROJAN CANDIDATES AND THE DISCOVERIES

In the selection of NT candidates, objects with semimajor axes in the range 29.7–30.3 au and $e < 0.3$ were chosen from the Outer Solar System Pipeline. They must have at least four "tracklets," and two of the four must have three detections or more. Therefore, to reach our minimal criteria, at least 10 detections must be spread over four different nights, and the total observational arc lengths must be longer than 1 yr. For example, the rediscovered NT 2011 QR_{322} just passed our minimal criteria: it has a pair detection in 2012 October, has two triplet detections separated in different nights of 2013

October, and has the other pair of detections in 2013 November.

Because of the long observational arc lengths, all candidates have fairly well determined orbital elements. One thousand clones of each candidate were generated from the orbit-fitting covariance matrix generated by the *orbfit* code of Bernstein & Khushalani (2000). From the 1000 clones we select the following three to be numerically integrated for 10 Myr: the best fit, the smallest semimajor axis, and the largest semimajor axis. If any of the three clones exhibits dynamical coupling with Neptune with the resonant argument, $\phi_{1:1}$, ~60° or 300°, they will be classified as a candidate NT. Note that the resonance argument, $\phi_{1:1} = \lambda_N - \lambda_T$, is defined by the difference of the mean longitude of Neptune (λ_N) and that of the Trojan candidate (λ_T) with $\lambda = M + \Omega + \omega$, where M is the mean anomaly, Ω is the longitude of the ascending node, and ω is the argument of perihelion.

Once the candidates have been identified, we checked whether they have been detected by the Dark Energy Survey (Dark Energy Survey Collaboration et al. 2016) or not. We also used the CADC SSOIS system (Gwyn et al. 2012) to examine whether the candidates have been observed in other archival data. One of the NTs, 2011 SO_{277}, was observed by the Dark Energy Survey, and another one, 2010 TT_{191}, was observed by the Canada–France–Hawaii Telescope (CFHT) in 2007. We also carried out follow-up observations at the predicted locations to confirm their existence using the Fred Lawrence Whipple Observatory 1.2 m, Lulin Observatory 1 m, and Lijiang 2.4 m telescopes of the Yunnan Astronomical Observatory. We used the astrometric data from these confirming observations to improve the orbital solutions. The same numerical procedure described above for the Trojan candidate identification was repeated.

We identified seven NTs, with most of the detections being contributed by the PS1 Solar System Survey. Figure 2 shows their spatial distribution, and the corresponding discovery/rediscovery latitude and longitude in ecliptic coordinates can be found in Table 1. The L5 region overlapped significantly with the Galactic center during the related observations. Two of the seven NTs are known L4 NTs, 2001 QR_{322} and 2006 RJ_{103}. For the other five newly discovered Trojans, one is located at L5 and the other four at L4. The detailed observation log can be found in the Minor Planet Center database.

4. ORBITAL AND PHYSICAL PROPERTIES

Table 1 summarizes the orbital elements of the NTs detected by PS1, including the two known ones, namely, 2001 QR_{322} and 2006 RJ_{103}. The PS1 detections along with previous observations were used to improve the orbital elements of these two objects. It is noted that the L5 Trojan, 2013 KY_{18}, has a relatively large eccentricity ($e \sim 0.12$), indicating the possibility of long-term orbital instability.

To understand the orbital properties and resonant behaviors of these Trojan candidates, we produced 1000 clones for each Trojan candidate covering the error ellipse of its orbital elements. That is, the initial orbital elements of each clone were generated from a multivariate normal distribution with the six-dimensional covariance matrix provided by the observation fitting routine, i.e., the *Orbfit* code of Bernstein & Khushalani (2000). Forward integration was performed for each clone over a time interval of 1 Gyr using the `Mercury 6.2` *N*-body code of Chambers (1999). As heliocentric orbital elements are used as the standard input to `Mercury 6.2`, the *orbfit* code has been modified to generate heliocentric orbital elements and the corresponding covariance matrix.

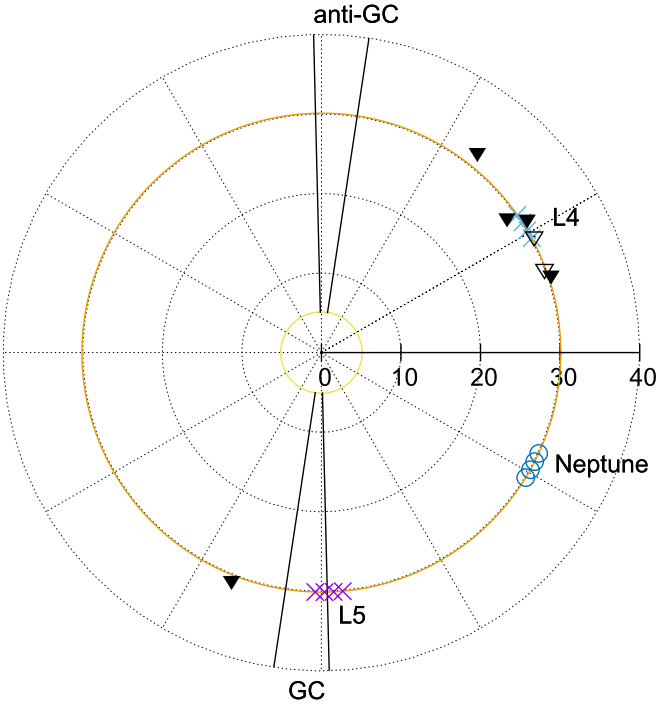

Figure 2. Spatial distribution of all PS1-detected Trojans. The filled triangles are the newly discoveried NTs, and open triangles are the known ones detected by PS1. The positions of NTs correspond to their first detections of PS1. The blue circles show the locations of Neptune from 2010 to 2013, and the crosses show the corresponding Lagrange points. Notice that the Galactic center (GC) overlapped with L5 during 2010–2012.

Table 2 shows the mean orbital elements, half-peak rms libration amplitudes, libration periods, and lifetimes of the seven NTs. These orbital parameters were computed from the numerical results of the first 100 Myr of the orbital integration except for 2013 KY_{18}, where the numerical values were derived from the first million years due to its short dynamical lifetime.

Our calculations show that most of the L4 NTs, except 2001 QR_{322}, have a half-life longer than 1 Gyr. For example, all of the clones of 2011 WG_{157}, 2010 TS_{191}, and 2006 RJ_{103} remained stable during the entire 1 Gyr orbital integration. Conversely, 2011 SO_{277} and 2010 TT_{191} lost about 100 (10%) and 300 (30%) clones, respectively. The known NT, 2001 QR_{322}, was found to have a half-life of about 0.53 Gyr, which agrees well with the previous result of about 0.55 Gyr from Horner & Lykawka (2010). The only L5 Trojan, 2013 KY_{18}, has a short half-life of about 3.2 Myr, which is similar to the value of less than 1 Myr of another unstable L5 Trojan, 2004 KV_{18} (Guan et al. 2012; Horner et al. 2012). This suggests that 2013 KY_{18} is likely to be a temporarily captured Trojan. Figure 3 shows the variations in resonant argument, $\phi_{1:1}$, of 2011 WG_{157} (top), 2001 QR_{322} (middle), and 2013 KY_{18} (bottom), which represent stable, marginally stable, and unstable NTs, respectively.

5. INCLINATION DISTRIBUTION OF STABLE L4 NTs

From the dynamical stability test described in Section 4, six of the seven NTs have half-lifetime longer than 0.5 Gyr. That

Table 2
Barycentric Orbital Properties of PS1-detected Neptune Trojans

Name	$\langle a \rangle$[a] (au)	$\langle e \rangle$	$\langle i \rangle$ (deg)	Libration Ampl. (deg)	Libration Per. (yr)	Half-lifetime
2001 QR_{322}	30.107 $\pm$[b] 0.122	0.030 ± 0.009	1.90 ± 0.82	27.3 $\pm$[c] 0.1	9268 ± 0	0.53 Gyr
2006 RJ_{103}	30.106 ± 0.027	0.025 ± 0.008	6.76 ± 1.12	5.6 ± 0.2	8858 ± 3	>1 Gyr
2010 TS_{191}	30.106 ± 0.056	0.047 ± 0.008	5.11 ± 1.11	12.1 ± 0.6	8896 ± 11	>1 Gyr
2010 TT_{191}	30.107 ± 0.091	0.068 ± 0.008	5.93 ± 1.10	19.9 ± 1.2	9040 ± 30	>1 Gyr
2011 SO_{277}	30.107 ± 0.089	0.016 ± 0.006	7.84 ± 1.16	19.7 ± 1.9	9104 ± 51	>1 Gyr
2011 WG_{157}	30.106 ± 0.068	0.027 ± 0.009	23.11 ± 1.12	15.6 ± 0.1	9458 ± 4	>1 Gyr
2013 KY_{18}	30.107 ± 0.095	0.106 ± 0.008	4.70 ± 0.98	20.8 ± 1.6	9023 ± 44	3.2 Myr

Notes.
[a] Mean elements, libration amplitude, and libration period were calculated from the results of forward 10 Myr integrations, except 2013 KY_{18}, which was calculated from the results of forward 1 Myr integrations.
[b] $\pm$ of mean *a, e, i* are the half-peak rms.
[c] $\pm$ of libration amplitude and libration period were calculated from the standard deviations from 1000 clones.

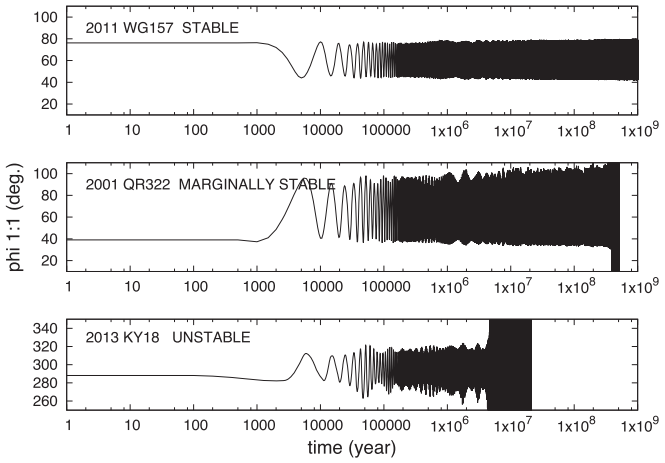

Figure 3. Resonant argument variations of 2011 WG_{157} (top), 2001 QR322 (middle), and 2013 KY_{18} (bottom). These represent three types of orbital stability, namely, stable, marginally stable, and instable NTs, respectively.

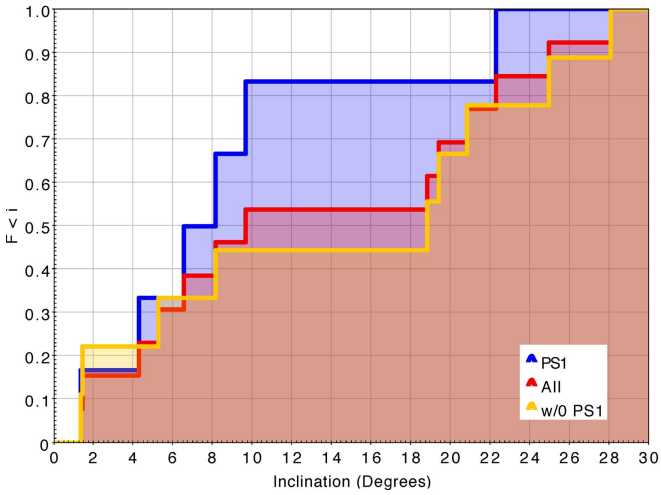

Figure 4. Cumulative inclination distributions of NTs for PS1 detected only (blue), all known Trojans included (red), and excluded PS1 discoveries (yellow). We find that (1) there are no NTs with $10^\circ < i < 18^\circ$ and (2) the PS1 NTs have a low-inclination distribution.

is, they belong to the stable population. Figure 4 shows the cumulative inclination distribution of those six objects. Two things are noticeable: (1) the presence of a bimodal inclination distribution without stable L4 TNs with inclinations between 10° and 18°, and (2) the NTs detected by PS1 display a rather low inclination distribution.

Parker (2015) first suggested that the inclination distribution of NTs might exhibit a bimodal structure from the observational point of view. This bimodal inclination distribution may have a dynamical origin. Zhou et al. (2009) demonstrated that the equality between the frequencies of $f_{2N:1U} - 2f_\sigma$ and the fundamental secular frequency g_6 can cause an instability, and its effective region crosses 15° in inclination when $a \sim 30.1$ au. Here $f_{2N:1U}$ is the frequency of the quasi-2:1 mean motion resonance between Neptune and Uranus, and f_σ is the libration frequency. This dynamical effect could explain our observations of a lack of stable Trojans between $i = 10^\circ$ and 18°.

In our PS1 survey, we have detected only one stable L4 Trojan with inclination greater than 20° and observed a rather low inclination distribution of NTs. To compare our observational result with the intrinsic inclination distribution estimated in Parker (2015), we would have to debias the PS1 survey data. However, the complicated PS1 survey cadence and camera structure make a detailed study difficult at the present moment. In the following, a simplified procedure is used to estimate the survey bias in inclination space.

The point of the inclination debiasing is to estimate what fraction of objects can be found in the PS1 survey, with our search algorithm, for a given orbital inclination. While the limiting magnitude and detection efficiency function are sufficient, especially because the NT's orbits are approximately circular, the sky coverage and number of exposures are the key factors. Therefore, our approximate PS1 detection efficiency function was assumed to be a function of the number of total exposures in a given survey region; survey regions with more exposures will have higher detection rates. Thus, the PS1 survey has the highest detection rate within $\pm 10^\circ$ of the ecliptic plane and a lower detection rate in the region between 10° and 15° and between -10° and -15° above and below, respectively. To proceed, we first assume that the limiting magnitude is 22.5, and indeed all of the NTs were detected around the limiting magnitude. Second, the detectability of $m = 22.5$ is assumed to be 50%, and the filling factor is 70%. For an NT, we will therefore have a 35% chance to detect it. Third, we must detect an NT for at least 10 times before claiming that we have found it. This assumption is based on the simplified version of our detection criteria in Section 3. Hence, The PS1 detection efficiency function can be approximated as

Table 3
Parameters of Survey Simulations

Simulation ID	σ_i (deg)	$\sigma_{L_{11}}$(deg)	$\sigma_{L_{11t}}$(deg)	σ_e	σ_{e_t}	Efficiency Function
Control Set	11	10	35	0.044	0.12	$f_{\rm eff}(n)$[a]
$f_{\rm eff}(R)$	11	10	35	0.044	0.12	$f_{\rm eff}(R)$[b]
$\sigma_L = 16°$	11	16	35	0.044	0.12	$f_{\rm eff}(n)$
$\sigma_e = 0.07$	11	10	35	0.07	0.12	$f_{\rm eff}(n)$

Notes.
[a] Brightness-independent detection efficiency function (Equation (4)).
[b] Brightness-dependent detection efficiency function (Equation (8)).

the total sum of probability mass functions of binomial distribution:

$$f_{\rm eff}\left(n\right) = \sum_{i=10}^{n} \binom{n}{i} 0.35^{i} \times (1 - 0.35)^{n-i}. \quad (4)$$

Here n is the total number of exposures in a specific survey region, and i is the minimal number of detections required for finding an object in our detecting pipeline. For example, if a survey region has 20, 30, or 40 exposures, the detection efficiency will be ∼0.12, 0.64, or 0.94, respectively. Using this detection efficiency function along with the approximated sky coverage map of the PS1 Solar System Survey (see Figure 1), we would be able to compute the whole sky detectability of NTs in 1 square degree resolution.

Having estimated the PS1 detection efficiency function, we can use the survey simulator from the Outer Solar System Origins Survey (OSSOS; Kavelaars et al. 2009; Bannister et al. 2016) in combination with the NT population model given in Parker (2015), in which the intrinsic inclination (i) distribution is equivalent to a truncated Brown's distribution,

$$p(i) = \begin{cases} \sin(i)\exp\left(-\frac{1}{2}(i/\sigma_i)^2\right)di, & i < i_t \\ 0, & i \geqslant i_t, \end{cases} \quad (5)$$

the intrinsic libration amplitude (L_{11}) distribution is a truncated Rayleigh distribution,

$$p(i) = \begin{cases} L_{11}\exp\left(-\frac{1}{2}(L_{11}/\sigma_{L_{11}})^2\right)dL_{11}, & L_{11} < L_{11t} \\ 0, & L_{11} \geqslant L_{11t}, \end{cases} \quad (6)$$

and finally the intrinsic eccentricity distribution also follows a truncated Rayleigh distribution,

$$p(i) = \begin{cases} e\exp\left(-\frac{1}{2}\right)(e/\sigma_e)^2)de, & e < e_t \\ 0, & e \geqslant e_t. \end{cases} \quad (7)$$

Here i_t, L_{11t}, and e_t are the truncation points of the inclination, libration amplitude, and eccentricity distributions, respectively.

To investigate the correlation between σ_i and the detection efficiency function during the survey simulations, we first ran the simulator with two different detection efficiency functions: (1) our brightness-independent PS1 detection efficiency function, and (2) a double hyperbolic tangents brightness-dependent detection efficiency function (Petit et al. 2006):

$$f_{\rm eff}\left(R\right) = \frac{A}{4}\left[1 - \tan h\left(\frac{R - R_c}{\Delta_1}\right)\right]\left[1 - \tan h\left(\frac{R - R_c}{\Delta_2}\right)\right]. \quad (8)$$

Here A, R_c, Δ_1, and Δ_2 are the filling factor (or maximal efficiency), rollover magnitude (50% of the maximal efficiency), and widths of the two components, respectively. In this simulation, we set $A = 0.9$, $R_c = 22.5$, and Δ_1 and Δ_2 are 0.01 and 0.15, respectively. We also made the similar procedure but with different $\sigma_{L_{11}}$ and σ_e. The parameters of each simulation are shown in Table 3, and the results of the simulated biased inclination distributions were shown in Figure 5.

The results clearly show that changing $\sigma_{L_{11}}$ or σ_e or using a different detection efficiency function does not affect the simulated biased inclination distributions. Therefore, to test the intrinsic inclination distribution, we set the σ_i from 5° to 21° with 1° steps and fixed the $\sigma_{L_{11}}$, $\sigma_{L_{11t}}$, σ_e, and $\sigma_{e_t}$to be 10°, 35°, 0.044, and 0.12, respectively, as suggested by Parker (2015) in our simulations.

To compare the simulation results with our observations, we computed the ratio of the high-i ($i > 18°$) to low-i ($i < 10°$) NTs from the simulation results and estimated the probability to generate the high-i/low-i ratio equal to 1/5 that was obtained from the PS1 survey. The criterion of the low and high$i$ follows from the fact that currently there are no known NTs within the 10°–18° inclination range.

The results are shown in Figure 6. The shaded areas show the 68% confidence (1σ) and 95% confidence (2σ) intervals. The cases of $\sigma_i > 27°$ and $\sigma_i < 7°$ would be rejected at 2σ level, and the most likely value is $\sigma_i \sim 11°$.

6. LUMINOSITY FUNCTION OF STABLE L4 NTs

Our approximate PS1 detection efficiency is a function of the total number of exposures in a specific survey region. For the NTs we found in the PS1 survey, the detection probabilities can be estimated from their detected coordinates. The detection probabilities of six L4 NTs are listed in Table 4.

We divided the L4 NT population into two bins, $H < 7.5$ and $H > 7.5$, and the density in each bin is the sum of the 1/prob. of every object in that bin, which is 2 and 7.18, respectively. The approximate slope, α, is $\log_{10}((7.18/2)/\Delta H)) \sim 0.86$, where ΔH is the H difference between two bins. This result shows that our rough debiasing produces a slope consistent with the values from Sheppard & Trujillo (2010a) and Fraser et al. (2014).

7. DISCUSSION

Parker (2015) suggested that if the stable NT cloud follows an inclination distribution similar to that of the Jovian Trojan population, the corresponding inclination width must be greater than 11°. Our result, which is based on six stable L4 NTs, is roughly consistent with his finding. Note that our most likely value of $\sigma_i \sim 11°$ is the minimal acceptable value in Parker

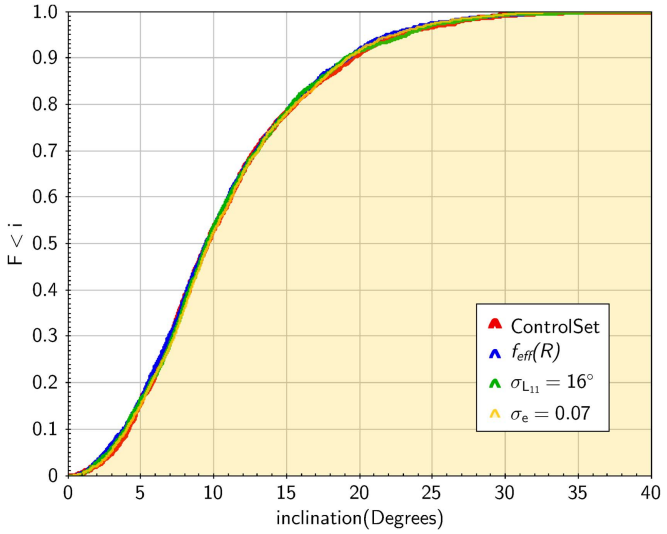

Figure 5. Simulated biased inclination distributions with different detection efficiency function or NT population model parameters. The results show that the simulated biased inclination distribution is independent of these factors.

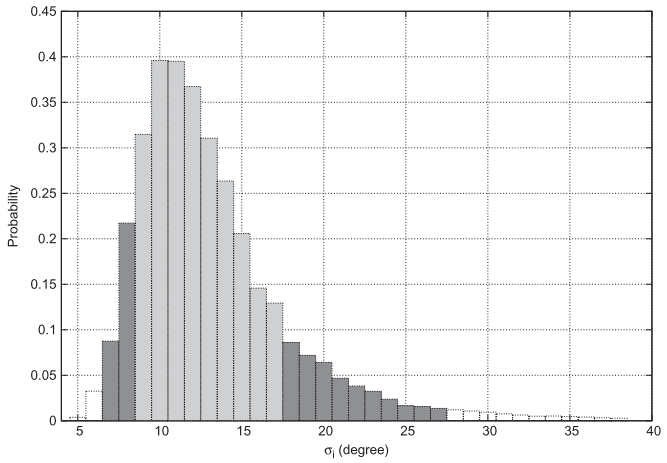

Figure 6. Probability distribution of NT inclination width parameter σ_i. Here the probability is the chance to reproduce high-i/low-i = 1/5 with specific σ_i. The shaded areas illustrate the 68% ($9° \leqslant \sigma_i \leqslant 17°$) and 95% ($7° \leqslant \sigma_i \leqslant 27°$) confidence intervals determined directly from the distribution.

Table 4
Detection Probabilities of Six L4 NTs

Name	H	Prob.	1/Prob.
2001 QR_{322}	7.9	1	1
2006 RJ_{103}	7.5	1	1
2010 TS_{191}	7.9	0.45	2.2
2010 TT_{191}	7.9	0.365	2.74
2011 SO_{277}	7.6	0.8	1.25
2011 WG_{157}	7.0	1	1

(2015). Therefore, our present result might be indicative of a lower inclination distribution.

It is worth noting that a high and wide NT inclination distribution with $\sigma_i \sim 20°$ is unlikely to result from capture from a dynamically cold disk without orbital damping during planet migration. However, the scenario is possible if the actual NT inclination distribution has σ_i only around 10° (Nesvorný & Vokrouhlický 2009; Parker 2015; Chen et al. 2016).

One other fact that should be taken into consideration is that the PS1 survey can only detect larger NTs ($H \lesssim 8$) compared to the other surveys with fainter limiting magnitudes. It may be the case that large and small NTs have different high/low-i ratios: if the NT cloud actually has cold and hot populations like the classical Kuiper Belt and the two populations have different size distributions, it might also explain the inconsistent measurements of the high/low inclination ratio.

Parker (2015) and Chen et al. (2016) simulated the captured NTs after planet migration and found that there is no difference between the numbers of captured L4 and L5 Trojans. The PS1 survey should not have any bias to detect high-eccentricity objects in the L4 region. However, we did not detect any unstable L4 NTs with high eccentricity. In the near future, as the L5 region moves away from the Galactic center, we will be able to test the possible asymmetry between the L4 and L5 populations. The ongoing PS1 + PS2 survey would be able to cover more than ±20° above and below the ecliptic plane and will be very useful in deriving a less biased inclination distribution of NTs. In addition, the future LSST survey will detect many more NTs, allowing a more nuanced understanding of their distribution to be gained.

8. SUMMARY

We report the detection of seven NTs in the PS1 Outer Solar System Survey. Five of these are new discoveries, consisting of one L5 Trojan and four L4 Trojans. Our numerical integrations show that the new L5 Trojan can be stable for only 3.2 Myr, and suggest that it is a temporarily captured object. The four new L4 Trojans can remain stable for over 1 Gyr and could be members of a primordial population. Only one stable L4 Trojan with inclination higher than 20° was detected by the PS1 survey. Our survey simulation results show that if the L4 NT cloud follows an inclination distribution similar to that of the Jovian Trojan population, at >95% confidence, it should have an inclination width, σ_i, between 7° and 27°. We suggest that the most likely value of σ_i is 11°, which corresponds to the minimal accepted value of σ_i from Parker (2015). Compared to previous surveys that discovered other known NTs, PS1 can only detect relatively large ($H \lesssim 8$) objects. Thus, the possible inconsistency between Parker (2015) and our result could hint at a size-dependent inclination distribution of NTs.

We would like to thank Zhong-Yi Lin and JianGuo Wang for observing with the YAO 2.4 m telescope. We are grateful to Mike Alexandersen for providing the Neptune Trojan population model of the OSSOS survey simulator. We are grateful to Gareth Williams of the Minor Planet Center for his ongoing help.

This work was supported in part by MOST Grant MOST 104-2119-008-024 (TANGO II), MOST Grant MOST 105-2112-M-008-024-MY3, MOE under the Aim for Top University Program NCU, and the Macau Technical Fund: 017/2014/A1 and 039/2013/A2. H.W.L. acknowledges the support of the CAS Fellowship for Taiwan-Youth-Visiting-Scholars under grant no. 2015TW2JB0001.

The Pan-STARRS 1 Surveys (PS1) have been made possible through contributions from the Institute for Astronomy, the University of Hawaii, the Pan-STARRS Project Office, the Max-Planck Society and its participating institutes, the Max Planck Institute for Astronomy, Heidelberg and the Max Planck Institute for Extraterrestrial Physics, Garching, Johns Hopkins University, Durham University, the University of

Edinburgh, Queen's University Belfast, the Harvard-Smithsonian Center for Astrophysics, the Las Cumbres Observatory Global Telescope Network Incorporated, the National Central University of Taiwan, the Space Telescope Science Institute, the National Aeronautics and Space Administration under grant no. NNX08AR22G issued through the Planetary Science Division of the NASA Science Mission Directorate, the National Science Foundation under grant no. AST-1238877, and the University of Maryland.

Facilities: PS1, CFHT, Blanco, FLWO:1.2m, YAO:2.4m, LO:1m.

Software: orbfit (Bernstein & Khushalani 2000) and Mercury 6.2 (Chambers 1999).

REFERENCES

Alexandersen, M., Gladman, B., Kavelaars, J. J., et al. 2014, arXiv:1411.7953
Bannister, M. T., Kavelaars, J. J., Petit, J.-M., et al. 2016, AJ, 152, 70
Bernstein, G., & Khushalani, B. 2000, AJ, 120, 3323
Brasser, R., Mikkola, S., Huang, T.-Y., Wiegert, P., & Innanen, K. 2004, MNRAS, 347, 833
Brown, M. E. 2001, AJ, 121, 2804
Chambers, J. E. 1999, MNRAS, 304, 793
Chen, Y.-Y., Ma, Y., & Zheng, J. 2016, MNRAS, 458, 4277
Chiang, E. I., & Lithwick, Y. 2005, ApJ, 628, 520
Dark Energy Survey Collaboration, Abbott, T., Abdalla, F. B., et al. 2016, MNRAS, 460, 1270
Dvorak, R., Schwarz, R., Süli, Á., & Kotoulas, T. 2007, MNRAS, 382, 1324
Elliot, J. L., Kern, S. D., Clancy, K. B., et al. 2005, AJ, 129, 1117
Fraser, W. C., Brown, M. E., Morbidelli, A., Parker, A., & Batygin, K. 2014, ApJ, 782, 100
Gerdes, D. W., Jennings, R. J., Bernstein, G. M., et al. 2016, AJ, 151, 39
Gomes, R., Levison, H. F., Tsiganis, K., & Morbidelli, A. 2005, Natur, 435, 466
Guan, P., Zhou, L.-Y., & Li, J. 2012, RAA, 12, 1549
Gwyn, S. D. J., Hill, N., & Kavelaars, J. J. 2012, PASP, 124, 579
Horner, J., & Lykawka, P. S. 2010, MNRAS, 405, 49
Horner, J., & Lykawka, P. S. 2012, MNRAS, 426, 159
Horner, J., Lykawka, P. S., Bannister, M. T., & Francis, P. 2012, MNRAS, 422, 2145
Kaiser, N., Burgett, W., Chambers, K., et al. 2010, Proc. SPIE, 7733, 77330E
Kavelaars, J. J., Jones, R. L., Gladman, B. J., et al. 2009, AJ, 137, 4917
Lee, C.-H., Riffeser, A., Koppenhoefer, J., et al. 2012, AJ, 143, 89
Lykawka, P. S., Horner, J., Jones, B. W., & Mukai, T. 2009, MNRAS, 398, 1715
Lykawka, P. S., Horner, J., Jones, B. W., & Mukai, T. 2011, MNRAS, 412, 537
Marzari, F., Tricarico, P., & Scholl, H. 2003, A&A, 410, 725
Morbidelli, A., Levison, H. F., Tsiganis, K., & Gomes, R. 2005, Natur, 435, 462
Nesvorný, D., & Dones, L. 2002, Icar, 160, 271
Nesvorný, D., & Vokrouhlický, D. 2009, AJ, 137, 5003
Parker, A. H. 2015, Icar, 247, 112
Parker, A. H., Buie, M. W., Osip, D. J., et al. 2013, AJ, 145, 96
Petit, J.-M., Holman, M. J., Gladman, B. J., et al. 2006, MNRAS, 365, 429
Sheppard, S. S., & Trujillo, C. A. 2006, Sci, 313, 511
Sheppard, S. S., & Trujillo, C. A. 2010a, ApJL, 723, L233
Sheppard, S. S., & Trujillo, C. A. 2010b, Sci, 329, 1304
Tonry, J. L., Stubbs, C. W., Lykke, K. R., et al. 2012, ApJ, 750, 99
Tsiganis, K., Gomes, R., Morbidelli, A., & Levison, H. F. 2005, Natur, 435, 459
Yoshida, F., & Nakamura, T. 2005, AJ, 130, 2900
Zhou, L.-Y., Dvorak, R., & Sun, Y.-S. 2009, MNRAS, 398, 1217
Zhou, L.-Y., Dvorak, R., & Sun, Y.-S. 2011, MNRAS, 410, 1849